Res. Chem. Intermed., Vol. 30, No. 4–5, pp. 459–488 (2004)

Also available online - www.vsppub.com

Review

Photochromism in transition-metal oxides

TAO HE and JIAN-NIAN YAO *

Key laboratory of Photochemistry, Center for Molecular Sciences and Institute of Chemistry, Chinese Academy of Sciences, Beijing 100080, P. R. China

Received 10 December 2004; accepted 14 January 2004

Abstract—Transition-metal oxides — including tungsten oxide, molybdenum oxide, titanium dioxide, vanadium pentoxide, niobium pentoxide and zinc oxide — exhibit photochromism upon bandgap excitation. These oxides constitute an important group of inorganic chromogenic materials, which is of great significance in the perspective of science and technology. During the past several decades, great progresses have been made in the microstructure, photochromic behavior and mechanism of these oxides, specifically of tungsten oxide. These studies underscore the opportunity of using these materials in photonic applications. The details will be presented in this review.

Keywords: Photochromism; transition-metal oxides; tungsten oxide; molybdenum oxide; titanium dioxide; vanadium pentoxide; niobium pentoxide; zinc oxide.

INTRODUCTION

Upon bandgap irradiation, electron-hole pairs can be generated in semiconductors of transition-metal oxides (TMOs). Depending on the behavior of these newly photo-generated electrons and holes, optical absorption of these TMOs may be changed obviously after the photo-excitation, leading to the changes in color. Such changes in color of TMOs upon light irradiation make them promising for a variety of applications in the fields of large area display, smart window, optical storage media, optical signal processing, chemical sensors, and so on.

At the early stage of the researches 'phototropy' [1] was introduced to designate this phenomenon and then 'photochromism' [2]. The first phenomenological observation of photochromism was from some paints containing zinc oxide based pigment, which dates back to the 19th century [3, 4]. About 70 years ago Parmelee and Badger [5] noted the color change of titanium dioxide-containing materials when exposed to visible or ultra-violet (UV) light. After Deb's pioneering

*To whom correspondence should be addressed. E-mail: jnyao@iccas.ac.cn

work [6–8], WO_3 and MoO_3 have received extensive attention among the photochromible TMOs. In addition, it is reported that V_2O_5 and Nb_2O_5 also show photochromism. Photochromic TMO materials have the advantages of high resistance to corrosion and heating. During the past several decades, great progresses have been achieved on the researches of these materials. The microstructure, photochromic behavior and mechanism of TMOs have been well studied. In the mean time, the photochromic response of TMOs has been extended from UV light to visible light [9, 10], which is of great significance for the efficient utilization of solar energy and lasers.

In the present paper, the studies on the photochromism of TMOs are reviewed. These TMOs include tungsten oxide, molybdenum oxide, titanium dioxide, vanadium pentoxide, niobium pentoxide and zinc oxide. The emphasis is put on the photochromic behavior and mechanism of tungsten oxide, which is the most thoroughly investigated chromogenic TMO and possibly the most promising candidate for practical applications.

TUNGSTEN OXIDE

Tungsten oxide (WO_3) is yellowish to greenish in bulk form. Its crystal structure is of perovskite-like (ReO_3 structure), which can be visualized as an infinite framework of corner-sharing WO_6 octahedra each with a central tungsten ion surrounded by six almost equidistant oxygen ions [11–15]. Tungsten oxide has a tendency to form substoichiometric (Magnéli) phase with edge-sharing octahedra and extended tunnels with large pentagonal or hexagonal cross-sections. Amorphous WO_3 (a-WO_3) is suggested to be a spatial network of tightly bounded clusters that are built from hydrated WO_6 octahedra sharing their corners or edges [16–18]. In a molecular model [11–13, 19–21], it consists of trimeric W_3O_9 molecules produced during the deposition, which can form three-member rings of octahedra and further six-member rings bound to each other through water-bridge, hydrogen and van der Waals bonding. Unlike the crystal, structure of WO_3 thin film exhibits only some short-range order. Granqvist [11–13] argued that a WO_3 film should be viewed as a nanocomposite — rather than a truly amorphous material — with a grain size between approx. 1 nm and approx. 5 nm, depending on the deposition conditions.

Photochromic behavior

The bandgap for tungsten oxide ranges from 2.6 to 3.4 eV [13], depending greatly on the preparation and post-treatment conditions. Upon bandgap irradiation, it can be switched reversibly from transparent to a blue colored state. A longer irradiation time will result in a larger photochromic response [22]. This photochromic phenomenon is observed most prominently in thin films of tungsten oxide [8, 22–70], which can be prepared by thermal evaporation [8, 26–28, 44, 45, 47, 48, 68, 71],

reactive evaporation [44, 72] rf sputtering [22, 29, 37, 44, 71], dc sputtering [54], electron beam deposition [34, 60], sol–gel-related techniques [24, 38, 55, 73, 74], spray pyrolysis [47], electrodeposition [63, 64], laser-related deposition technique [51, 52, 58] and so on. Different techniques for the film preparation often lead to thin films with somewhat different properties. WO_3 powder [35, 39, 75] and colloids [38, 76–83] also show coloration upon the bandgap excitation. In addition, laser irradiation (308 nm) can induce chemical reactions in solids, leading to the formation of substoichiometric WO_3 [84–87]. Although WO_3 turns to a deep blue or blue-black color too, it should be ascribed to the thermochromism not photochromism [84–87]. This is similar to the case in which WO_3 is heated in vacuum [23]. A similar phenomenon has also been observed in CeO_2, TiO_2, Nb_2O_5, MoO_3, etc. [84, 85].

Figure 1 shows the UV-Vis absorption spectra of the virgin and colored WO_3 films. A broad absorption band with a maximum at *ca.* 910 nm appears with one shoulder towards the visible range and another at *ca.* 1600 nm. The main absorption edge can be separated into two parts. In the first part with the absorption coefficient (α) less than 10^4 cm^{-1}, the absorption edge is an exponential function of photon energy, which is similar to the Urbach's edges in a number of amorphous and crystalline materials. The origin of this exponential tail absorption probably arises from the random fluctuation of the internal fields associated with structural disorder, which is considerable in an amorphous solid [88]. In the second part with α larger than 10^4 cm^{-1} the absorption edge follows the relation, $(\alpha h\nu)^{1/2}$ *vs.* hν–Eg, where Eg is defined as the optical energy gap. The high absorption coefficient (approx. 10^5 cm^{-1}) and the square-law dependency of the absorption coefficient on photon energy suggest that the absorption in this region be contributed to the allowed direct (momentum conserved) band to band transition [8], which probably arises from some localized states at the top of the valence band to extended states above the mobility edge in the conduction band. The fact that the absorption spectrum of

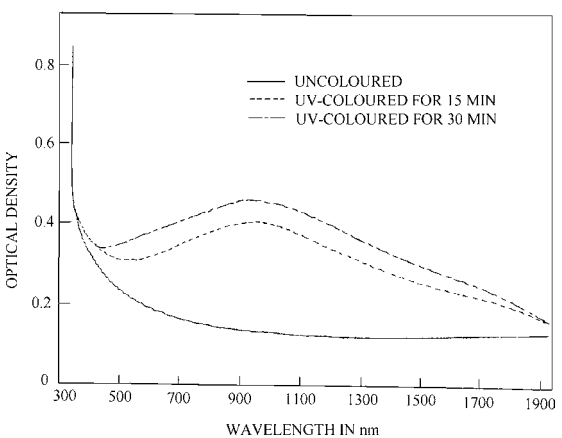

Figure 1. Absorption spectra of amorphous WO_3 films (adapted from Ref. [8]).

a crystalline film is essentially similar to that of the amorphous film, except for a lateral shift in energy of the absorption edge, argues that the essential feature of the band structure is retained in the amorphous phase [8]. The color remains quite stable in an inert atmosphere and there is a slight optical bleaching (5%) upon visible light irradiation. The color can be bleached by the introduction of oxidizing agent (such as O_2, O_3, H_2O_2 and $Fe_2(SO_4)_3$) [8, 23, 26, 33, 35, 36, 48], by application of anodic polarization [63, 64], or by heating treatment in air [8]. In the case of bleaching by oxidizing agent or anodic polarization, the film can be colored again by UV light irradiation. However, in the last case the coloration efficiency is progressively reduced until the film is fully oxidized in which case no coloration is observed [8].

Besides the UV-Vis absorption spectra, the virgin and colored WO_3 films have been characterized widely by many other techniques, such as electron spin resonance (ESR) [73], Raman spectroscopy [17, 60], Fourier transform infrared (FT-IR) absorption spectra [24, 60, 73], X-ray photoelectron spectroscopy (XPS) [45, 50, 58, 63, 64], extended X-ray absorption fine-structure spectroscopy (EXAFS) [73], X-ray diffraction (XRD) [8, 24], electron diffraction [8], electron microscopy [8, 24, 38, 73], atomic force microscopy (AFM) [58], scanning tunneling microscopy (STM) [58], Auger electron spectroscopy (AES) [50], small-angle X-ray scattering (SAXS) [38, 73], ellipsometry [54], electrical characterization [8, 28, 44, 58], etc. These results indicate that the UV-light irradiation can lead to lots of changes in the properties of WO_3 as well as the coloration. For instance, electrical conductivity [8, 28, 44, 58] and photoconductivity [8] of WO_3 films increase greatly after the photo-excitation. During the photochromic process film strains are observed in WO_3 film due to the insertion of protons [22].

Photochromic mechanism

Several theoretical models have been put forward to explain the formation of the optical absorption band in photo-colored tungsten oxide. The observed structure in the absorption spectrum should be an intrinsic property of WO_3 since the absorption coefficient (10^5 cm^{-1}) is too high to be attributed to any impurity [8]. In addition, it cannot be ascribed to the charge transfer absorption from the oxygen valence band to a 'split-off' W^{5+} state, which is similar to the bandgap absorption but occurs at a lower energy [89].

Deb [8] has attributed the photochromic effect of WO_3 film to the absorption of F-like color centers when he observed this phenomenon first. WO_3 thin film contains oxygen vacancies, which are present as a result of the deposition process. These positively charged defects can trap photo-excitated electrons, resulting in the formation of F-like color centers. The excited state of the F-center is assumed to be located below the conduction band by an amount greater than kT that accounts for the inefficient photo-bleaching of the color center at common temperature. The protons act as charge compensating ions to the injected electrons. Bleaching in an oxidizing atmosphere could be attributed to direct annihilation of ground state trapped electrons by the oxidizing species. Since the sample has a very high

absorption coefficient (10^5 cm^{-1}) at the wavelength responsible for coloration, the color centers are generally formed in a very thin layer (100 nm) on the surface. Consequently the density of centers (concentration of optical centers) must be quite large so as to produce an obvious change in optical density, which is estimated to be 10^{19}–10^{20} cm^{-3} by Smakula's equation. But some authors argued that such a high density of color centers made it unlikely to arise from oxygen vacancies [89]. Moreover, very little conclusive evidence exists for the observation of F and F^+ optical bands in oxides other than alkaline earth oxides [90]. In addition, electrons 'trapped' by oxygen vacancies are likely to reside on tungsten orbitals with optical properties fitting into the transition of intervalence charge transfer or small polaron [89].

After the foundation of connection between optical modulation and a double insertion/extraction of ions and electrons [89, 91], many authors started to use it to elucidate the photochromic mechanism of tungsten oxide although it is developed from the electrochromism. The key point here is the formation of hydrogen tungsten bronze and the theoretical modeling is focused on an intervalence charge transfer (IVCT) mechanism or on a closely related mechanism based on small polaron absorption. Upon bandgap irradiation electrons and holes are produced in WO_3 (equation (1)). The photo-generated electron is injected into the conduction band and is trapped at a W^{6+} site to give a W^{5+} color center; while the hole reacts with the adsorbed H_2O to produce protons simultaneously (equation (2)), which subsequently diffuse into WO_3 lattice. Thus hydrogen tungsten bronze ($H_xW^{VI}_{1-x}W^{V}_xO_3$) is formed (equation (3)). The resulting W^{5+} states after the coloration has been confirmed by XPS and ESR experiments, which are situated at approx. 0.8 eV below the Fermi level [33, 35, 36, 45]. In addition, the photo-generated electrons can recombine with the holes (equation (4)), which is detrimental to the photochromism. According to IVCT mechanism, the intervalence charge transfer or *d–d* transition from the newly formed W^{5+} (valence band-like) to adjacent W^{6+} (conduction band) site results in the blue color of the film. This requires largely 'delocalized' electrons with some overlap between metal ions [89, 91]. In addition, since electrons and holes are produced by a photoelectrochemical process instead of electric power, some authors [30, 46, 75, 76, 81, 83] have suggested the nomenclature to be photoelectrochromism.

$$WO_3 + h\nu \rightarrow WO_3^* + e^- + h^+ \tag{1}$$

$$2h^+ + H_2O \rightarrow 2H^+ + O \tag{2}$$

$$WO_3 + xH^+ + xe^- \rightarrow H_xW^{VI}_{1-x}W^{V}_xO_3 \tag{3}$$

$$h^+ + e^- \rightarrow \text{heat} \tag{4}$$

The small-polaron theory [71, 92] is similar to the IVCT model except that the shift in the energy peak upon crystallization and the asymmetry of the high-energy side of the optical absorption in amorphous films has led to the postulation

of a self-trapping (disorder) term in the expression for the energy peak, which lowers the energy of the site with the trapped electron relative to other W^{6+} sites. Since not all W^{6+} sites have equivalent energy in a disordered system, the injected electrons will be trapped primarily in those sites with the lowest energy and polarize their surrounding lattice to form small polarons [93, 94]. At the same time, wave functions for the neighboring sites become overlapped. Incident photons are absorbed by small polarons, and the optical absorption of the colored film is a result of the small-polaron transitions through hopping between two neighboring non-equivalent sites of tungsten (equation (5)). Hence, optical transitions can be acquired with a range of energies, which explains the shift to lower energy for crystalline films and the asymmetry in the optical-absorption width. It is noted that at room temperature small-polaron properties are found only in amorphous materials [92]. Thus, the problem for this model is that in real systems whether the electron actually distorts the lattice around the tungsten ion to further lower its energy by forming a bound polaron.

$$W_A^{VI} + W_B^{V} \xrightarrow{h\nu} W_A^{V} + W_B^{VI} \tag{5}$$

Although it seems not yet possible to discriminate in a meaningful way between the prediction from IVCT and small-polaron theory, Granqvist [13] suggested that the latter might be the 'correct' one for the disordered tungsten oxide. He elucidated the coloration and decoloration of the film based on the fact that the color of a chemical species is closely related to the configuration and behavior of electrons. The valence band of WO_3 is a p band arising form the overlapping of the O_{2p} orbitals, and the conduction band is assumed to be a d band arising from the W_{5d} orbitals [13, 14, 33, 45]. It should be noted that the W_{6s} state also contributes to the conduction band. But it does not contribute to the coloration process, since no electrons will be excited into this level upon light irradiation. The d levels are split into e_g and t_{2g} levels (by means of the conventional notations) (Fig. 2), while the O_{2p} orbital is split into $2p_\sigma$ and $2p_\pi$. The incipient molecular energy levels are broadened into bands in the perovskite lattice. Since there are 24 electrons in the shown bands for WO_3, the Fermi level lies in the gap between t_{2g} and p_π band. The bandgap is wide enough to render the material transparent. Upon bandgap irradiation, electrons will transfer from p_π to t_{2g} bands and the Fermi level moves upwards in the presumed rigid-band scheme. Since the oxide film is heavily disordered, the excess electrons and their lattice polarization can hop from one ion site to another by absorbing a photon so that the materials exhibit polaron absorption. The peak absorption lies in the near infrared, which renders the oxide bluish. Once the electrons 'go back' to p_π bands, it returns to the original transparent state. So tungsten oxide is a 'reductive' photochromic material.

Notwithstanding the aforementioned models based on the formation of tungsten bronze are consistent with many experimental observations, they cannot explain the following results. (1) Once the color centers are bleached by heating in an oxygen atmosphere, the oxide cannot be colored again by bandgap irradiation [8]. (2) The

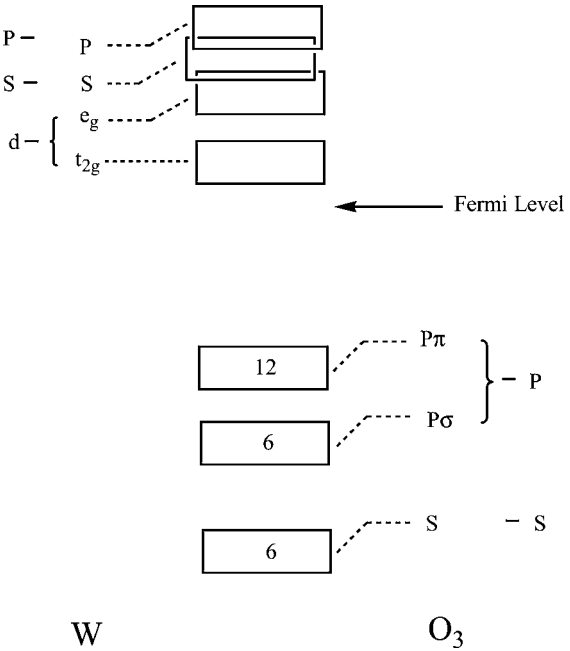

Figure 2. Schematic band structure for WO_3. The incipient atomic and molecular levels are shown by using standard notation. The numbers in the different bands denote electron capacities (adapted from Ref. [12]).

coloration efficiency of tungsten oxide films (WO_{3-x}) increases with increasing oxygen deficiency (x) [26, 27, 29, 54]. (3) The potential is insufficiently negative for the photo-generated electrons to reduce tungsten oxide to the hydrogen tungsten bronze [79, 82, 95]. Since there is no bias applied and no external charges injected during the coloration process, it might be unsuitable to simply 'copy' the whole mechanism derived from the electrochromism for photochromism although sometimes it is claimed that they are identical [39]. Therefore, some authors [26, 27, 29, 96] go back again to the oxygen defects for the answer.

A typical as-deposited tungsten oxide film has tungsten mainly in the W^{6+} and W^{4+} states and the number of W^{4+} states increases with increasing oxygen deficiency in the virgin samples [13, 19, 29, 96]. Although several groups [45, 71, 97] have claimed the existence of W^{5+} in as-deposited films, most of these data are for the films colored by various post-treatment methods. No ESR signal of W^{5+} is found in either crystalline WO_3 (c-WO_3) or as-evaporated a-WO_{3-x} ($0 \leqslant x \leqslant 0.4$) films [44, 98], while this signal increases with increasing coloration in the post-treated films. Some authors [44, 99] have used the pairing of W^{5+} polarons to explain this discrepancy. They suggested the coloration originate from local transfer of hydrogen from passive sites to active sites within the material. The ionization of hydrogen occurs during this transfer process, which supplies the electrons needed for the increase in the concentration of W^{5+} ions. If W^{5+} is present

in the as-deposited film, however it cannot be explained why in most cases the film is colorless if the color is caused by the transition between W^{5+} and W^{6+} states. Since tungsten oxide film always possesses certain amount of water, it can be represented as ${W_{1-x}}^{6+}{W_x}^{4+}O_{3-x}nH_2O$, where n is the amount of water bonded in the film structure [96]. The incorporated water increases in concentration in amorphous films as the oxygen deficiency increases [26, 27, 54]. The photochromic reactions in $WO_{3-x}nH_2O$ film are thus expressed as follows:

$$\begin{aligned} WO_{3-x}nH_2O + h\nu &= {W_{1-x}}^{6+}{W_x}^{4+}O_{3-x}nH_2O + h\nu \\ &= {W_{1-x}}^{6+}{W_x}^{4+}O_{3-x}(n - y/2)H_2O + yH^+ + ye^- + (y/2)O \end{aligned} \tag{6}$$

$$\begin{aligned} &{W_{1-x}}^{6+}{W_x}^{4+}O_{3-x}(n - y/2)H_2O + yH^+ + ye^- + h\nu \\ &\quad = {W_{1-x-y}}^{6+}W{y}^{5+}{W_x}^{4+}O_{3-x-y/2}nH_2O = WO_{3-x-y/2}nH_2O \end{aligned} \tag{7}$$

The protons in equation (6) result from the oxidization of adsorbed water by holes. The oxygen radicals may temporarily occupy the oxygen vacancies inside the sample (for a relatively thick film) or escape as molecular oxygen into the atmosphere (for a considerably thin film) [26, 27, 29], which would also prevent the back-reaction of equation (6). Thereafter the separated protons will combine with some O^{2-} in the film to form H_2O with the help of photon energy (equation (7)). It is noted that equation (7) is similar to that proposed by Chang *et al*. [100] for the electrochromism of WO_3, in which extraction of oxygen from WO_3 leads to colored decomposition compounds of general formula WO_{3-x}:

$$WO_3 + 2xH^+ + 2xe^- \rightarrow WO_{3-x} + xH_2O. \tag{8}$$

Thus, the net photochromic reaction is

$$WO_{3-x}nH_2O + 2h\nu = WO_{3-x-y/2}nH_2O + (y/2)O \tag{9}$$

This means that the photochromic reaction will be faster in an oxygen-free environment and slower in an oxygen-rich environment, as observed by some authors [26]. It indicates that the oxygen deficiency in a tungsten oxide film is increased while the number of water molecules in the film keeps unchanged during the photochromic reaction. This accounts for a high density of color centers in the colored species. It can also explain the photochromic efficiency increases with increasing oxygen deficiency in tungsten oxide. Moreover, bleaching to the original absorption state only occurs if oxygen is offered to the sample from outside (equation (10)). Otherwise, the decay of color centers remains incomplete until the ambient atmosphere is changed to O_2 [26]. The proposed chromic mechanism [96] is based on the small polaron transition between the charge-induced W^{5+} state and the original W^{4+} state instead of the W^{5+} and W^{6+} states as suggested in previous models. Here one should distinguish the following differences: (a) the original oxygen deficiency and charge-induced oxygen deficiency and, (b) the original lower valence tungsten state and charge-induced lower valence tungsten state. It is noted that, in electrochromism of

WO_3, Ozkan *et al.* [101] suggested that the optical absorption is the result of small polaron transition between W^{5+} and W^{4+} states and between W^{5+} and W^{6+} states.

$$WO_{3-x-y/2}nH_2O + (y/4)O_2 = WO_{3-x}nH_2O \tag{10}$$

In addition, for both the colloids [76, 79, 81, 83] and particulate films [30, 46, 61], some authors suggested the absorption should come from the trapped electrons and few [82] claimed the absorption to be caused by free carriers. It is proposed that the electrons are trapped at the metal ion sites at the surface vacancies [76, 81, 83, 102]. These trapped electrons are stable in an inert atmosphere and can be used as the storage of light energy, which might be released in the dark for a special utilization (such as the reduction of dyes with less negative reduction potentials than the conduction band of WO_3) [76, 78, 83]. Also, the formation of neither the tungsten bronze nor the F-like centers is preferred in this mechanism. Here one should also note the differences between the absorption of free and trapped electrons. Free electrons produce free-carrier absorption at longer wavelengths and the corresponding molar absorption coefficient increases continuously with wavelength ($\varepsilon \sim \lambda^n$) and linearly with carrier concentration, while trapped electrons generally display an absorption maximum [82, 102–105]. However, if the electron is trapped in a shallow level, the absorption maximum may be in the far-infrared where competitive absorption by the solvent or substrate makes detection difficult. Therefore, the observation of an increasing absorptivity in the visible and near-IR regions may lead to the false conclusion that free carriers are present, when in fact an absorption maximum is present at lower energies. Moreover, free-carrier absorption is associated with a more crystalline structure, while the trapped-electron absorption occurs mainly in an amorphous structure.

In summary, although some controversies still remain among different authors, almost all the experimental results can be explained by at least one of the aforementioned mechanisms. The question is that there is always one peak with at least one shoulder appearing in the absorption spectrum. One can always observe slight differences, oftentimes large differences, in the peak position and/or the shape of the absorption spectra for different films even under the same coloration protocol. This means, although all the films display blue color, it might be unsuitable to attribute only a single origin to such bands. Thus, this asymmetric absorption curve should be interpreted to be a superposition of many discrete bands, which might result from different transitions as supposed by some authors [106, 107].

Influence factors of the photochromism

There are many factors that can influence the photochromic behavior of tungsten oxide. The structure and composition of tungsten oxide film are responsible for the optical characteristics, which strongly depend on the preparation methods as well as the treatment conditions [34, 38, 54, 57, 72]. The basic structural unit of the amorphous and crystalline thin films of tungsten oxide is the WO_6 octahedron. The

optical properties strongly rely on whether the WO_6 octahedra are alone [72, 108] or linked with other octahedra through the corners [72, 109] or edges [72, 110]. In the case of an isolated octahedron the optical absorption spectra of reduced tungsten ions consists of two weak *d–d* transitions and an absorption edge above 4 eV [72, 108]. In the case when the octahedra are linked by corners the absorption edge moves to smaller energies and in the case of c-WO_3 appears as a non-direct allowed transition at 2.7 eV [16, 72], but in case of a-WO_3 as a modified direct allowed transition at 3.4 eV [8, 16, 72].

Heat pretreatment will affect the crystalline of WO_3 film and lead to the changes in its photochromism. The as-deposited film is usually amorphous and may become crystalline after annealing at a high temperature. If the film is deposited onto a heated substrate, the crystalline structure can also be obtained for the newly prepared film. The absorption peak of the film is shifted to a higher energy side with increasing annealing temperature and then shifted abruptly to a lower energy as the film starts to crystallize [72, 101]. It has been reported [8, 34, 47] that the amorphous films show faster photochromic response (or better photochromism) than the polycrystalline ones probably due to the difference in the fine structure, particularly to the number of lattice defects. However, Cikmach *et al.* [72] argued that the coloring efficiency in the amorphous state is the same as that in the oriented polycrystalline state. Shigesato [60] claimed that the film that has a higher density and lower crystallinity of framework structure shows lower saturated photochromism. The former is due to a smaller amount of the adsorbed species available for UV desorption kept by a denser film, whereas the latter is due to increases in the optical gap caused by decreased size of the microcrystals [111] or decreases in the amount of adsorbed water in the film with low crystallinity [60]. It has been reported that WO_3 nanoparticles show better photochromic response than the corresponding bulk material [51, 52] and the colloids of smaller particles present better color changes [76].

The photochromic properties of tungsten oxide are very sensitive to the composition of the surrounding atmosphere during the illumination [39, 40]. The role of O_2 has already discussed in previous parts, which can bleach the colored film at ambient atmosphere. This is a substantial problem for the application of photochromism to an optical memory device. Another important factor is the adsorbed molecules that can act as the proton donors. As mentioned above, the generation of protons is of great importance in the coloration process. When molecular proton donors (such as water and reducible small organic molecules containing oxygen atoms) are adsorbed on the surface of WO_3 films, the protons can be generated as a result of oxidation of these molecules by photo-generated holes. Many authors have investigated their influences on the photochromic response of WO_3 films.

Adsorbed water plays an important role in the photochromic reaction as discussed above. The as-prepared film contains three kinds of adsorbed water on the surface or interior: physically adsorbed water, chemisorbed water and structural water [60, 112–114]. The former two kinds of water show no influence on the photochromic

properties, whereas the last does show the influence [60, 112, 115]. During the photochromic process, the adsorbed water not only affords the counter ions (protons) for coloration, but also provides a high ionic conductivity [113, 116, 117] and stabilizes active surface sites [113]. The acceleration of hydrogen movement is explained by the formation of chains of OH and OH_2 groups in the tungsten network, and the hopping of hydrogen particles between adjacent oxygen and hydroxyl groups [117, 118]. Although WO_3 exhibits better photochromism in a humid environment than in a dry environment [8, 96], one should note that tungsten oxide film can undergo photocorrosion reactions if too much water is adsorbed on the surface or WO_3 is put in water or aqueous solution (equations (11) and (12)) [119, 120].

$$WO_3 + 2h^+ + 2H_2O \rightarrow WO_4^{2-} + 4H^+ + \frac{1}{2}O_2 \tag{11}$$

$$H^+ + e^- \rightarrow \frac{1}{2}H_2 \tag{12}$$

It is found that the photochromism of WO_3 will be improved when it is illuminated in the vapor of alcohols or organic acids [37, 39–43, 47, 68–70, 75, 119, 121]. Similar to the adsorbed water, these small molecules can react with the photogenerated holes to produce protons sometimes accompanied with the evolution of CO_2 gas [75, 121]. However, unlike the adsorbed water [26, 27, 54], in case of these organic molecules the presence of oxygen vacancies raises the Fermi level, leading to the reduction of photoinjection efficiency of hydrogen [43]. It is reported [43, 107] that film evaporation in organic vapor drastically enhances the surface area, which in turn enhances the photochromic sensitivity of the film. In addition, Dinh *et al*. [34] claimed that WO_3 films can also show photochromism when they are put in a solution of formic acid or dehydrated $LiClO_4$/propylene carbonate. The blue color of the film colored in $LiClO_4$/PC is much more stable in the air than that colored in formic acid. This is due to the formation of more stable lithium tungsten bronze similar to that formed in the electrochromism [13].

It has been reported [39, 40] that a texture with (001) orientation for polycrystalline WO_3 films is extremely favorable for the photoinjection of hydrogen because this plane has a high free energy. Another reason is that there are two types of channels in WO_3 crystals, both of which are perpendicular to the (001) plane, which coincide with the direction of proton diffusion [39, 40, 122]. In addition, since organic molecules prefer to be adsorbed on the surface of amorphous layer, a double-layer heterostructure consisting of polycrystalline and amorphous tungsten oxide has been fabricated [41–43]. First the hydrogen is injected into the amorphous layer and then migrates into the polycrystalline layer. Thus the photoinjection of hydrogen into polycrystalline tungsten oxide is improved.

Visible light coloration induced by cathodic polarization

The photochromic sensitivity of WO_3 is limited to the energies above its bandgap, corresponding to the near-UV range. For efficient utilization of solar energy and laser sources that cover a broad wavelength from mid-IR to blue, it is meaningful to extend the coloration response to the visible-light region [123, 124]. The pretreatment of cathodic polarization in K^+/propylene carbonate solution can induce the visible-light coloration in WO_3 [70, 125]. First WO_3 thin films are slightly colored by cathodic polarization in KNO_3/propylene carbonate solution. The subsequent irradiation with visible light in 0.05% (v/v) ethanol/N_2 produces a strong color enhancement (Fig. 3). This visible-light colored film is fairly stable if it is not exposed to the atmosphere containing oxidant. It is suggested [125] that this color enhancement is related to the formation of K_xWO_3 during the polarization. The resulting K_xWO_3 can induce slight deformation in oxide microstructure and produce metastable trap states with energy levels lying inside the bandgap region. These newly formed intermediate states are accessible to the visible light, leading to the reactions as the same as those induced by UV-light and hence the visible-light coloration. It should be noted that visible-light coloration is observed only with films slightly pre-colored by cathodic polarization (with the formation of alkali bronze), not by bandgap irradiation (with the formation of hydrogen bronze). The injected cations for these two processes are K^+ and H^+, respectively. Although during the photochromic process film stress is observed in WO_3 film due to the insertion of protons [22], the radius of proton is too small to cause enough changes in oxide structure that can produce the intermediate states accessible to the visible light, or such kind of change corresponding to the strains are inaccessible to the

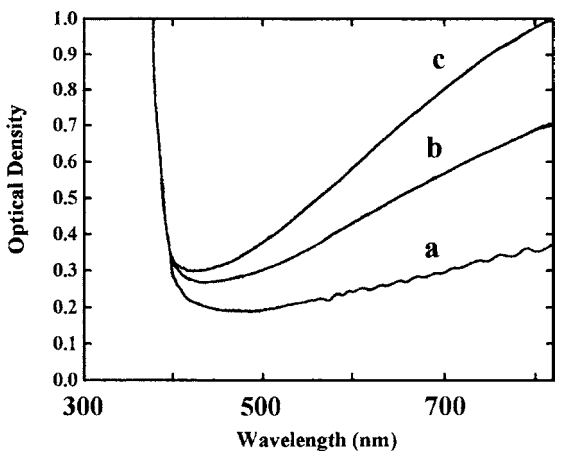

Figure 3. Optical densities of a WO_3 thin film. Curve a, WO_3 thin film as prepared by vacuum evaporation; curve b, spectrum taken after the sample was polarized cathodically at 0.05 mA/cm^2 for 12 mC in a 0.1 mol/l KNO_3/propylene carbonate solution; curve c, spectrum taken after the sample in b was irradiated with visible light ($\lambda \geqslant 500$ nm) for 40 min in 0.05% (v/v) ethanol/N_2 (after Ref. [125]).

visible light. The radius of alkali ions is large enough to produce such kind of states [125].

MOLYBDENUM OXIDE

Photochromic behavior and mechanism

Molybdenum oxide (MoO_3) is another kind of TMO that shows pronounced photochromism and has many, though not all, properties in common with tungsten oxide. The bulk crystal of molybdenum oxide has an orthorhombic structure (α-phase), which consists of corner-sharing chains of MoO_6 octahedra that share edges with two similar chains to form layers of MoO_3 stoichiometry [11–13]. These layers are stacked in a staggered arrangement and are only held together by weak van der Waals forces. The most interested molybdenum oxide in this review has a monoclinic structure (β-phase), which is of the perovskite-like type, and can be regarded as a metastable analogue of WO_3. In between these octahedra there are extended tunnels that can serve as conduits and intercalation sites for mobile ions. MoO_3 thin films are similar to those of WO_3, which has the structure of perovskite-like type built by corner-sharing MoO_6 octahedra [11–13, 18, 126].

The commercial molybdenum oxide is white or light grey colored powder. Amorphous MoO_3 films exhibit better photochromic responses than crystalline films [127] or single crystals [128] and, thus, are more suitable for construction of photonic devices [127]. AFM observations show that amorphous MoO_3 films are composed of grains ranging from 100 to 190 nm in size, which is made up of smaller particles approximately 25 nm in diameter [129]. MoO_3 film can be prepared by thermal evaporation [6, 7, 9, 18, 68, 128–135], flash evaporation [136], rf sputtering [126, 127], dc sputtering [137], electron-beam evaporation [138, 139], chemical vapor deposition [140–142], sol–gel-related techniques [74, 143, 144], electrodeposition [145, 146], thermal decomposition of MoS_3 [147], laser-related deposition [51, 52, 148], and so forth. Also, different preparation technique often leads to somewhat different properties.

The bandgap for MoO_3 ranges from 2.7 to 3.2 eV [124, 126–128, 130], depending greatly on the preparation conditions as well as the treatments. Similar to WO_3, if the transparent virgin MoO_3 film is irradiated by light with the energy above the bandgap, it turns blue and a very broad asymmetric absorption band develops accordingly with a peak in the near-IR region and a shoulder towards the visible range (Fig. 4). The asymmetric absorption curve has been interpreted to consist of a superposition of many discrete bands [6, 92, 128]. The photochromic response grows rapidly during the early stage of irradiation and then becomes saturated. The colored films can be bleached thermally in presence of oxygen but not by optical irradiation at their absorption maxima [6, 7]. However, as in the case of WO_3 [8], once the film is bleached thermally in oxygen, it cannot be colored again by photo-irradiation. The film bleached by anodic polarization can be colored again by

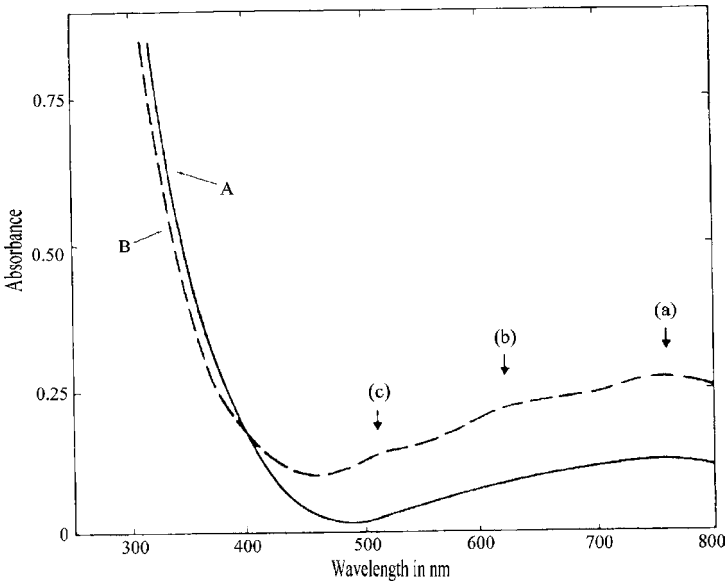

Figure 4. Absorption spectra before and after UV irradiation of MoO_3 thin film. (A) as-deposited film; (B) after UV irradiation showing three absorption peaks at (a), (b) and (c) (after Ref. [6]).

UV-light irradiation, demonstrating the reversibility of the coloration/decoloration cycle [68]. The origin of the absorption band for colored molybdenum oxide is very similar to that for tungsten oxide [124]. One is due to the formation of F-like color centers [6, 7]; another is the IVCT [89, 91] or small polaron absorption [13, 92] based on the double insertion/extraction of ions and electrons [89]. For the details, please see the section on the photochromic mechanism of tungsten oxide.

Virgin and colored MoO_3 films have also been widely characterized by some physical techniques, such as AES [137], AFM [129, 148], ESR [6, 7, 131, 149–152], FT-IR absorption spectra [132, 142, 148], SAXS [38], XPS [33, 35, 36, 133, 135, 148, 153], XRD [7, 126, 137, 140, 142, 148, 154–157], electrical characterization [6, 138, 139, 149, 158], electron diffraction [6, 7, 137], energy dispersive spectrometer (EDS) [137], neutron diffraction and scattering [155], Raman spectroscopy [53, 159–161], scanning electron microscopy (SEM) [38, 126, 138–140, 142], UV-Vis absorption spectra [6, 7, 9, 51, 52, 56, 68, 126–128, 130, 140, 141, 145, 148, 156, 162–165], and so on. The same as WO_3, UV-light irradiation can lead to lots of changes in the properties of MoO_3 films. For example, the electrical conductivity [6, 134, 149] and photoconductivity [157] of MoO_3 films increase greatly after the UV-light irradiation. The disorder increases in the structure of amorphous MoO_3 as a result of the UV-induced coloration, and decreases in the bleaching process [159]. It is also claimed that a similar grain structure (roughly the same size, shape and density) is observed for the as-grown and photochromic states [129].

Influence factors of the photochromism

Many factors can influence the photochromic performance of molybdenum oxide. The optical properties of molybdenum oxide are strongly dependent on the method used for the film preparation and are sensitive to the morphology of the film [38]. The vacuum evaporated film exhibits a better reversibility than the electrodeposited film, whereas the latter presents a larger photochromic response than the former [145]. For amorphous oxide film, the increase in the photochromic sensitivity with increased film thickness terminates when the light-penetration depth in the film reaches *ca.* 1 μm [166]. The amorphous film shows better photochromic response than that of crystalline film [127, 128]. Moreover, neither the single crystals of molybdenum oxide nor thin films prepared by sublimation in air can be colored upon exposure to UV light [128]. It has been reported [51, 52] that MoO_3 nanoparticles show a stronger photochromic effect than the corresponding bulk material, and experience photochromism even upon exposure to the normal room light.

The effects of oxygen on the photochromism of MoO_3 are identical to those of WO_3, although the bleaching speed in air is much slower for the colored molybdenum species [26–28, 68]. Under the same experimental conditions, MoO_3 film exhibits the best photochromic response under vacuum, followed in air and in oxygen [68]. MoO_3 film also shows better photochromism in N_2 atmosphere than in air [143].

Similar to WO_3, the proton donors (such as H_2O, C_2H_5OH and CH_3OH) adsorbed on the surface of MoO_3 film can be oxidized by holes and thus facilitate the photoreduction of MoO_3 by photoinjection of protons into the film [68, 167, 168], resulting in improved photochromic sensitivity [68–70, 106, 143, 144, 157, 167–169]. However, it should be noted that, like WO_3, the amorphous MoO_3 film can dissolve easily even in pure water due to the formation of soluble MoO_4^{2-} [139]. The effects of alcohols are dependent on the stability of the resulting radicals, the size of alcohol molecules, adsorption enthalpy or the molar mass of alcohols [47, 68, 143]. This can explain why the change in absorption due to photochromism for evaporated MoO_3 films is the largest in C_2H_5OH vapor, followed by CH_3OH, n-$(CH_3)_2CHOH$ and i-$(CH_3)_2CHOH$. Similar phenomenon has also been observed in the WO_3 system [47]. In addition, it is claimed [68] that MoO_3 is sensitive to the presence of small amounts of C_2H_5OH and insensitive to the presence of HCOOH since the latter has a more positive redox potential than the former. On the basis of this observation, the chemical sensing for alcohol with photochromic thin films might be devised. The amorphous films modified with dimethylformamide during the evaporation possess significant photochromic sensitivity at low temperatures (35, 90, 200 and 300 K) in an inert atmosphere [106].

Visible light coloration induced by cathodic polarization

The photochromism of MoO_3 samples without any pretreatment can be induced only by UV light. About 10 years ago, the first observation of the photochromic

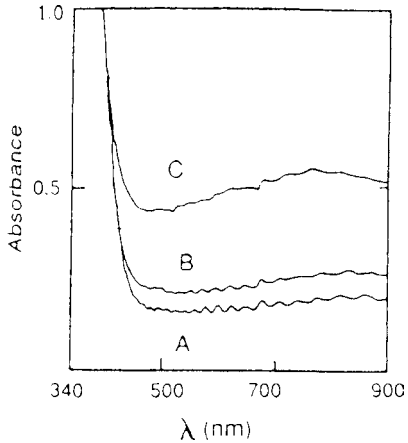

Figure 5. Absorption spectra of a MoO_3 thin film. (A) as prepared by vacuum evaporation; (B) spectrum taken after polarization at −0.1 V *vs*. Ag/AgCl for 3 min in 0.1 M $LiClO_4$/propylene carbonate solution; and (C) taken after the film in curve B was irradiated with visible light ($\lambda \geqslant$ 500 nm) for 10 min in air (after Ref. [9]). The sinusoidal modulation of the spectra is ascribed to the interference effects.

MoO_3 film induced by visible light was reported [9]. First, MoO_3 thin film is slightly blued by cathodic polarization in $LiClO_4$/propylene carbonate solution. The subsequent irradiation with visible light in air produces a strong color enhancement (Fig. 5). Similar color enhancement can also be observed even on near-infrared irradiation ($\lambda \geqslant$ 700 nm). This visible-light colored film is quite stable in air and the color enhancement is not caused by a thermal process [9]. The reason is just as the same as that for WO_3 system. Li_xMoO_3 is formed during the polarization, which can cause the structural deformation and are accessible to the visible light [9, 69, 70, 123, 146, 170–172]. Also, pretreatment of bandgap irradiation cannot induce visible-light coloration [9]. The blue color induced by visible light can be readily erased by anodic polarization, indicating the reversible coloration-decoloration cycle. Thus, a dual-mode display device is proposed with a combination of electrochemical mode and photon mode in MoO_3 thin films [9].

Memory effect induced by photo-irradiation

Another interesting phenomenon observed in MoO_3 thin film is the memory effect [69, 170]. One half of MoO_3 film is slightly subjected to UV-light irradiation in air, while the other half of the same sample is masked against irradiation. After the colored portion becomes colorless without heating in air, the whole sample is irradiated again with UV light. Compared with the non-exposed portion, the blue color of the pre-exposed half becomes much deeper. This means that the image acquired previously can be memorized, which is named the memory effect [69, 170]. This phenomenon is attributed to the different surface states on different portions of the same sample with and without the photo-irradiation pretreatment [124]. In addi-

tion, the increased conductivity [135, 173] and disorder [159] of the film after the pretreatment of UV-light irradiation might also contribute to this memory effect.

TITANIUM DIOXIDE

Photochromic behavior and mechanism

Bulk titanium dioxide (TiO_2) has different crystal structures at normal pressure, i.e., rutile, anatase and brookite. Rutile is thermodynamically more stable in structure than anatase, which is characterized by almost octahedral TiO_6 units forming a framework with infinite edge-shared chains and an equal number of vacant tunnels [11–13]. Anatase phase consists of infinite planar double chains of TiO_6 octahedra that are connected by corner-sharing [11–13], which has been extensively used for applications involving electron-transfer processes (such as photo-electrochemical energy conversion, photocatalysis and organic synthesis).

The bandgap of rutile and anatase TiO_2 is 3.00 and 3.23 eV, respectively. Single TiO_2 crystal does not show any appreciable photochromism at room temperature. However, at temperature lower than 77 K it shows photochromic properties similar to the alkali earth titanates [174]. Bandgap excitation of TiO_2 sol [103, 175–183], gel [182–186], powder [187, 188] and film [188, 189] in an oxygen-free atmosphere results in a photochromic response (blue in color). The colored TiO_2 cannot be bleached by visible laser excitation [184]. The colored species usually exhibit a broad of quasi-continuous featureless absorption in the wavelength domain between 450 and 1000 nm, which is associated with the behavior of electrons injected into TiO_2. It is noted that the maximum in the absorption spectrum ranges from 500 nm to 900 nm and sometimes no maximum is observed. This divergence can be rationalized by the optical properties of excess electrons in a semiconductor. The electrons injected into TiO_2 are either localized in traps or move freely in the conduction band (Fig. 6), depending on the crystal structure of TiO_2. The free-carrier absorption is associated with a crystalline structure, while the absorption of localized electrons mainly with an amorphous structure. The fact that the electronic spectra observed by most researchers exhibit a maximum rather than a continuously increasing absorption with wavelength, no matter where the centered position is, indicates that at least a part of the charge carriers are trapped. For the differences between the absorption of free and trapped electrons, please see the section on the photochromic mechamism of tungsten oxide. It should also be pointed out that the absorption of trapped holes, also observed by some authors, is at 475 nm [190].

Electrons are first excited to the conduction band and subsequently move to the trap sites. Although some authors [105, 180, 191] argued that electrons might be trapped at oxygen vacancies, it is generally accepted that the trapping sites are Ti(IV) sites locating at, or close to, the surface of TiO_2 particles or films [102, 105, 176, 181, 184, 187, 191] where most of the defects and impurities are present [105, 181]. The diffusion of electron–hole pairs to the surface of the

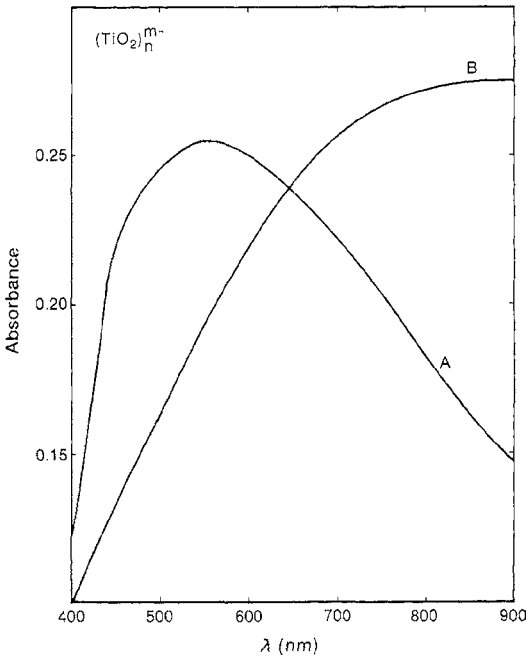

Figure 6. Absorption spectra obtained after γ-irradiation (3.5 kGy) of colloidal TiO_2 solutions in the presence of 0.1 M propanol-2 at pH 2. Colloids were prepared by different methods: (A) by dialysis of $TiCl_4$ solution at 0°C (TiO_2 total concentration of 0.125 M, 5-nm radius); (B) after 2 h of boiling $TiCl_4$ in acid solution (0.013 M concentration total, 50 nm radius) (after Ref. [103]). Curve A does not show characteristic absorption of free carrier, but rather a peak indicative of localized electrons. Curve B shows increased absorption with longer wavelengths above 400 nm, which is consistent with free carrier absorption.

colloidal particles is rapid in illuminated colloidal TiO_2 and the lifetime of charge carriers is less than 30 ns [176]. So the colored Ti^{3+} species are formed during the bandgap excitation, leading to the appearance of the absorption band. Highfield and Grätzel [187] suggested that this absorption band is the characteristic of small-polaron excitation (a bulk and/or surface Ti^{3+} center stabilized by an associated local anion distortion). The presence of Ti^{3+} species has been confirmed by the absorption spectroscopy and electron spin resonance measurements. As much as 10% of the available Ti^{4+} ions can be reduced photochemically in the solid of TiO_2 sol with a quantum yield of 3% under anoxic conditions [178]. It has been claimed [180] that the trapping of electrons as Ti^{3+} species is more efficient in smaller TiO_2 particles and a blue shift in the maximum occurs accordingly. In addition, it is found that in acidic solution all of the electrons are trapped as Ti^{3+}, whereas in alkaline solution only 10% of the electrons are detected as EPR-visible Ti^{3+} and the possibility of free electrons remaining untrapped cannot be discounted [102]. This might be due to that for the alkaline colloid the particle size is an order of magnitude larger and/or the surface trap sites in alkaline colloids are less efficient than those in acidic solution. The trapped electrons can be kept for months in the

absence of O_2 and no significant spectral changes are observed during the decay process. However, they are easily quenched in the presence of O_2. Similar to the case in WO_3, the trapped electrons in TiO_2 particles can be used for actinometry [177] or for the reduction of some organic molecules (such as textile azo dyes and obaltoceniumdicarboxylate) [83, 105].

If TiO_2 films are irradiated with UV light under vacuum, the absorption spectrum also shows a broad band, which displays a continuous rise beginning at 550 nm and extending into near-IR [192]. The dark blue color is stable under the vacuum but rapidly disappears upon exposure to air. O_2 is formed upon UV irradiation from either the photo-oxidation of adsorbed water or the creation of oxygen vacancies [192]. In the former case, the reaction can generate electrons in the conduction band and lead to the stabilization of photoinjected electrons and possible intercalation of protons into TiO_2 film. In the latter case, irradiating TiO_2 film under vacuum is expected to accelerate the creation of oxygen vacancies. It is also claimed [192] that the blue color appeared darker for TiO_2 films annealed at 200°C than for those annealed at 100°C due to the increased content and size of rutile crystallites.

Influence factors of the photochromism

Similar to WO_3 and MoO_3, improved photochromism of TiO_2 can be achieved by suppressing the recombination of photoexcited charge-carrier pairs. One possible way is to apply an external anodic bias [189]. The most-generally accepted method is to use the scavengers. Scavenging of photo-generated holes by suitable scavengers (such as water, alcohol, iodide and acetate) prevents them from recombining with the electrons and facilitates the accumulation of electrons, resulting in an intense blue color [83, 102, 105, 175, 177, 187–189, 192, 193]. It is found the presence of water vapor can extend the decay constants of recombination process from seconds to minutes [187]. Howe *et al.* [102] suggested that electron trapping occur at both surface and interior sites in the presence of a hole scavenger, while only at interior sites in the absence of a hole scavenger.

Matsumoto *et al.* [186] have reported that the degree of coloration and the recovery time for the monolithic gel of TiO_2 are strongly affected by the kind of salt catalysts although the color is independent. The active salt catalyst (such as hydrazine monohydrochloride) located around Ti ions enhanced the formation of the color center, Ti^{3+}. They argued that the mobility of proton through the active salt catalyst is indispensable for color development since no photochromism was observed in a xerogel. It seems that this might also be related to the effects of water in the (xero)gel.

Henglein [176] has reported that in acidic TiO_2 sols containing propanol-2 or ethanol the sols become blue at short irradiation times, and this color slowly disappears upon further irradiation; while this phenomenon cannot be observed in the sols containing methanol, t-butanol or benzene. Here the blue color is attributed to the highly active titanium-III-hydroxide formed in the electron transfer from organic radicals to TiO_2 colloidal particles (equation (13), where TiO_2^- is a blue

color center). Organic radicals are formed through the oxidation of alcohol by holes. So the overall reaction consists of the transition of titanium from colloidal state into solution and the rate of this dissolution is greater for the sol with smaller particles. The dissolution of TiO_2 under illumination has been reported by other authors [194]. The disappearance of the color centers upon longer irradiation is explained in terms of the destruction of trapping sites at which long-lived color centers can be formed, which occurs during the dissolution of the colloids.

$$(CH_3)_2\dot{C}OH + TiO_2 \rightarrow (CH_3)_2CO + TiO_2^- + H^+ \quad (13)$$

OTHER PHOTOCHROMIC TRANSITION-METAL OXIDES

Vanadium pentoxide

Vanadium pentoxide (V_2O_5) is an n-type semiconductor with a layered structure, which can be thought of as built from corner-sharing and edge-sharing VO_6 octahedra and is in this regard analogous to all of the other photochromic oxides mentioned above [195]. However, the deviation from the ideal octahedral positions is so large that it is more adequate to describe the structure in terms of layers of square pyramids of VO_5 units [11–13, 195]. V_2O_5 is special in that charge insertion makes the transmittance increase in the UV and short-wavelength parts of the luminous spectrum, while decrease in the long-wavelength part of this spectrum and in the near-IR [195]. This dichotomy motivates an in-depth examination of the coloration of V_2O_5 based films from a fundamental perspective and potential applications in multicolor display devices [195].

Several groups [10, 33, 196] have studied the photochromic behavior of V_2O_5. The thermal evaporated V_2O_5 films exhibit substantial absorption at energies below the optical width of the energy gap for V_2O_5 (Fig. 7), which stems from the large number of oxygen vacancies in the films produced by thermal evaporation in vacuum; this large number of vacancies leads in turn to tetravalent vanadium ions, V^{4+}, and to optical *d–d* transitions [10]. The absorption spectra indicate that irradiation shifts the intrinsic absorption edge of V_2O_5 to higher energies and a weak additional absorption appears in the visible region of the spectrum, which is typical for the photochromic effects in V_2O_5 layers and is associated with the formation of oxygen vacancies [10].

Nishio *et al*. [197, 198] have reported polycrystalline V_2O_5 turns blue-black upon irradiation with visible laser light (514.5 or 532 nm) in air due to the reduction of V^{5+}. They argued that this kind of coloration is induced by light, not by heat. It seems reasonable that this binary oxide can exhibit visible-light coloration since its optical bandgap falls into the visible range (520–580 nm) [10, 199, 200]. The problem is that the effects of heating cannot be ruled out in this case even according to the evidences given in these works. In addition, Sol and Tilley [84] have observed a dark silver-grey metallic appearance of V_2O_5 after the laser irradiation, which is ascribed to the thermochromism. So, more convincing evidence should be provided.

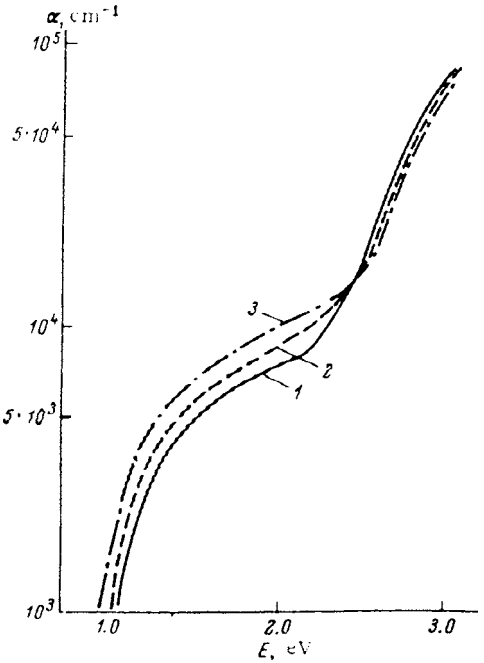

Figure 7. Spectrum of the absorption coefficient of V_2O_5 films during the photochromic process (after Ref. [10]). (1) Original film; (2) illumination for 1 h; (3) illumination for 4 h.

Interestingly, V_2O_5 gel displays another kind of absorption spectrum upon photoexcitation in methanol vapor (Fig. 8). Transparent V_2O_5 gel changes its color in methanol vapor from yellow to dark-green for thinner layers and from red to black for thicker layers [196]. Besides the aforementioned typical characteristics, a wide and structureless non-Gaussian absorption band with a maximum at 0.92 eV (1350 nm) appears. In addition, electrical conductivity of V_2O_5 gel increases with the irradiation time. The mechanism for the change in optical and electrical properties is similar to that for WO_3 and MoO_3 thin films [68, 173, 201], in which the formation of hydrogen oxide bronze is suggested (equation (14)) [196]. The protons result from the oxidation of adsorbed methanol by holes. However, V_2O_5 thin layers prepared by thermal evaporation do not become more photosensitive when irradiated in methanol vapor [196]. In order to have a relatively high hydrogen injection efficiency, it is claimed [196] that the V_2O_5 layer should have a large specific surface area, a large number of adsorption centers with intermediate Lewis acidity, a structure suitable for a rapid diffusion of hydrogen atoms through the entire thickness of the layer, and so on. V_2O_5 gel satisfies all these requirements, while the evaporated film does not.

$$V_2O_5 + xH^+ + xe^- \rightarrow H_xV_2O_5 \tag{14}$$

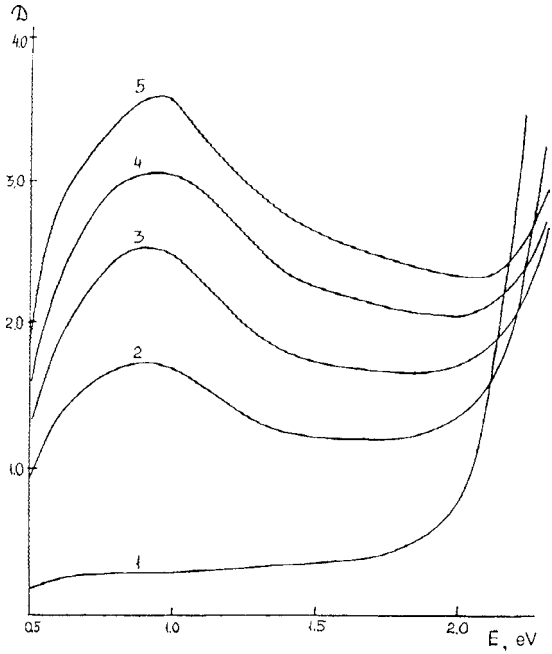

Figure 8. Spectral curves of the optical density D of V_2O_5-gel layers before and after UV irradiation: (1) before irradiation; (2) 30 min irradiation; (3) 1.5 h; (4) 3 h; (5) 5 h. The thickness of the layer is 5.5 μm (after Ref. [196]).

Niobium pentoxide

Niobium pentoxide (Nb_2O_5) is categorized as being of block-type, which exhibits both similarities and differences compared with ReO_3 and rutile structure [11–13]. Most phases of Nb_2O_5 comprise blocks of corner-sharing NbO_6 octahedra with a well defined cross section in one plane and infinite extent in the perpendicular direction. The blocks are connected by edge-sharing octahedra, yielding two sets of columns with different bases. Amorphous Nb_2O_5 (white color) thin film exhibits good photochromic response (blue color) in ethanol vapor (Fig. 9) and in N_2 atmosphere (Fig. 10), but not in air or in a pure O_2 atmosphere. The blue colored hydrogen niobium bronze ($H_xNb_2O_5$) can be formed by the reaction with H^+ and e^- (equation (15)) and be oxidized rapidly by O_2 (equation (16)). The protons can be provided from the oxidation of adsorbed ethanol or water. Although the photochromic response of Nb_2O_5 thin film is inferior to that of WO_3 or MoO_3, it could possibly be used in chemical sensing because Nb_2O_5 thin film, unlike WO_3 or MoO_3, shows no photochromism in the air (Fig. 10). This can result in reduction of the background noise [69, 70, 202].

$$Nb_2O_5 + xH^+ + xe^- \rightarrow H_xNb_2O_5 \tag{15}$$

$$4H_xNb_2O_5 + xO_2 \rightarrow 4Nb_2O_5 + 2xH_2O \tag{16}$$

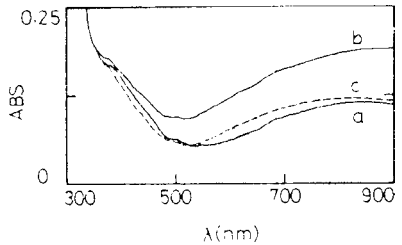

Figure 9. The photochromic responses of Nb_2O_5 thin film. (a) as-prepared by vacuum evaporation; (b) after the film in (a) was UV irradiated for 5 min in 3% C_2H_5OH/N_2 environment; (c) after the film in (b) was removed from the cell and left in the air for 1 h (after Ref. [202]).

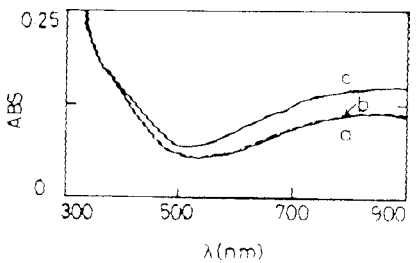

Figure 10. The photochromic responses of Nb_2O_5 thin film. (a) as-prepared by vacuum evaporation; (b) after the film in (a) was UV irradiated for 5 min in the air or in O_2; (c) after the film in (a) was UV irradiated for 5 min in N_2 (after Ref. [202]).

Zinc oxide

Pure zinc oxide (ZnO) is a finely divided white solid with the wurtzite structure. Few literatures are related to the photochromism of ZnO although, to some extent, it does exhibit this behavior. Figure 11 is the transient absorption spectra of colloidal ZnO suspension in ethanol. Similar to the case of TiO_2 colloids [179], the broad absorption in the red region is attributed to the electrons trapped at the surface of ZnO [203, 204]. The trapping of electrons is a fast process and completed within the duration of the laser pulse (18 ps). The trapped electrons can be quenched by O_2, N_2O and other electron scavengers. In addition, Matsuoka and Ono [205] have reported that abnormally oriented ZnO films prepared by sputtering-type electron cyclotron resonance microwave plasma can be darkened by X-ray irradiation (Fig. 12). Unlike the ZnO colloids, this kind of photochromism is ascribed to the oxygen vacancy in ZnO films, which strongly depends on crystallite orientation. The darkening cannot be observed in *c*-axis well-oriented films due to the few oxygen vacancies present in these systems. The better the abnormal-plane orientation is, the deeper the film is darkened by the X-ray irradiation.

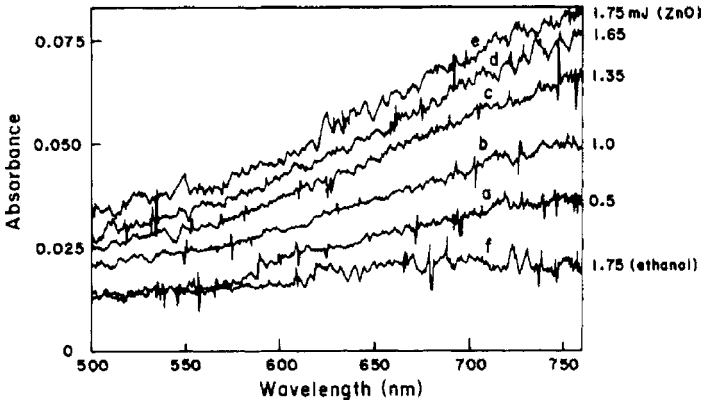

Figure 11. Absorption spectra recorded immediately after 355-nm laser pulse excitation ($\Delta t = 0$ ps) of 2 mM colloids in ethanol at various laser intensities: (a) 0.5, (b) 1.0, (c) 1.35, (d) 1.65 and (e) 1.75 mJ/pulse. Spectrum (f) represents blank ethanol excited with a 266-nm laser pulse at 1.75 mJ/pulse (after Ref. [203]).

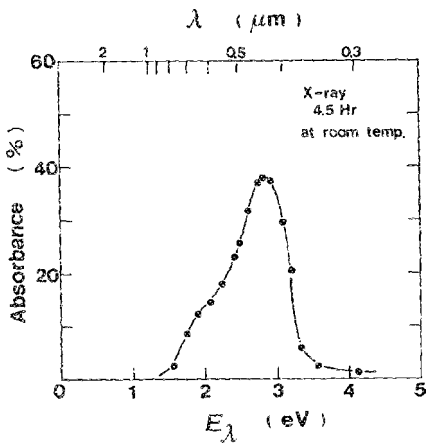

Figure 12. Typical absorption spectrum caused by color center in ZnO film with X-ray irradiation at room temperature. The film thickness is 0.08 μm (after Ref. [205]).

CONCLUSIONS

TMOs are an important group of inorganic chromogenic materials. During the past several decades, some significant progresses have been achieved, such as response to visible light, improved photochromism by proton donors, etc. Considering the photochromic mechanism of TMOs, one notes that this effect is mainly contributed by photo-induced reduction of TMOs or trapping of photo-generated electrons, and occasionally by oxygen vacancies. These studies underscore the opportunity of TMOs in photonic applications and may be useful for design of new inorganic photochromic materials, such as the composite and hybrid systems [79, 123, 167, 171, 206–210].

Acknowledgements

Financial support came from National Science Foundation of China, National Research Fund for Fundamental Key Projects No. 973 (G19990330), and Chinese Academy of Sciences.

REFERENCES

1. W. Marckwald, *Z. Phys. Chem.* **30**, 140 (1899).
2. R. Exelby and R. Grinter, *Chem. Rev.* **65**, 247 (1965).
3. L. Chalkley Jr., *Chem. Rev.* **6**, 217 (1929).
4. J. B. Orr, *Chem. News* **44**, 12 (1881).
5. C. W. Parmelee and A. Badger, *J. Am. Ceram. Soc.* **17**, 1 (1934).
6. S. K. Deb and J. A. Chopoorian, *J. Appl. Phys.* **37**, 4818 (1966).
7. S. K. Deb, *Proc. Roy. Soc. A* **304**, 211 (1968).
8. S. K. Deb, *Philos. Magn.* **27**, 801 (1973).
9. J. N. Yao, K. Hashimoto and A. Fujishima, *Nature* **355**, 624 (1992).
10. A. I. Gavrilyuk, N. M. Reinov and F. A. Chudnovskii, *Sov. Tech. Phys. Lett.* **5**, 514 (1979) (*Pis'ma Zh. Tekh. Fiz.* **5**, 1227 (1979)).
11. C. G. Granqvist, *Appl. Phys. A* **57**, 3 (1993).
12. C. G. Granqvist, *Solar Energ. Mater. Solar Cells* **32**, 369 (1994).
13. C. G. Granqvist, *Handbook of Inorganic Electrochromic Materials*. Elsevier, Amsterdam (1995).
14. M. Greenblatt, *Chem. Rev.* **88**, 31 (1988).
15. E. Salje and K. Viswanathan, *Acta Crystallogr. A* **31**, 356 (1975).
16. J. J. Kleperis, P. D. Cikmach and A. R. Lusis, *Phys. Stat. Sol. A* **83**, 291 (1984).
17. G. M. Ramâns, J. V. Gabrusenoks and A. Vespâls, *Phys. State Sol. A* **74**, K41 (1982).
18. G. M. Ramâns, J. V. Gabrusenoks, A. R. Lusis and A. A. Patmalnieks, *J. Non-Cryst. Solids* **90**, 637 (1987).
19. Y. A. Yang, Y. Ma, J. N. Yao and B. H. Loo, *J. Non-Cryst. Solids* **272**, 71 (2000).
20. J. Berkowitz, W. A. Chupka and M. G. Inghram, *J. Chem. Phys.* **27**, 85 (1957).
21. T. C. Arnoldussen, *J. Electrochem. Soc.* **128**, 117 (1981).
22. M. R. Goulding, C. B. Thomas and R. J. Hurditch, *Solid State Commun.* **46**, 451 (1983).
23. J. Scarminio, *Solar Energ. Mater. Solar Cells* **79**, 357 (2003).
24. A. P. Baker, S. N. B. Hodgson and M. J. Edirisinghe, *Surf. Coat. Tech.* **153**, 184 (2002).
25. K. Bange, *Solar Energ. Mater. Solar Cells* **58**, 1 (1999).
26. C. Bechinger, G. Oefinger, S. Herminghaus and P. Leiderer, *J. Appl. Phys*. **74**, 4527 (1993).
27. C. Bechinger, D. Ebner, S. Herminghaus and P. Leiderer, *Solid State Commun.* **89**, 205 (1994).
28. C. Bechinger, S. Herminghaus and P. Leiderer, *Thin Solid Films* **239**, 156 (1994).
29. C. Bechinger, M. S. Burdis and J. G. Zhang, *Solid State Commun.* **101**, 753 (1997).
30. I. Bedja, S. Hotchandani, R. Carpentier, K. Vinodgopal and P. V. Kamat, *Thin Solid Films* **247**, 195 (1994).
31. R. Bussjager, J. Chaiken, M. Getbehead, D. Grucza, D. Hinkel, T. McEwen, J. Osman and E. Voss, *Jpn. J. Appl. Phys. Part 1* **39**, 789 (2000).
32. A. Chemseddine, *J. Non-Cryst. Solids* **147**, 313 (1992).
33. R. J. Colton, A. M. Guzman and J. W. Rabalais, *Acc. Chem. Res.* **11**, 170 (1978).
34. N. N. Dinh, V. T. Bich, N. H. Hoang and L. Q. Minh, *Phys. Stat. Sol. A* **108**, K157 (1988).
35. T. H. Fleisch and G. J. Mains, *J. Chem. Phys.* **76**, 780 (1982).
36. T. H. Fleisch, G. W. Zajac, J. O. Schreiner and G. J. Mains, *Appl. Surf. Sci.* **26**, 488 (1986).

37. J. R. Galvao and J. Scarminio, *Quim. Nova* **26**, 488 (2003).
38. B. Sh. Galyamov, L. Yu. Mogilevskii and I. E. Obvintseva, *Rus. J. Phys. Chem.* **64**, 501 (1990).
39. A. I. Gavrilyuk, B. P. Zakharchenya and F. A. Chudnovskii, *Sov. Tech. Phys. Lett.* **6**, 512 (1980) (*Pis'ma Zh. Tekh. Fiz.* **6**, 1196 (1980)).
40. A. I. Gavrilyuk, V. G. Prokhvatilov and F. A. Chudnovskii, *Sov. Phys. Solid State* **24**, 558 (1982) (*Fiz. Tverd. Tela (Leningrad)* **24**, 982 (1982)).
41. A. I. Gavrilyuk, T. G. Lanskaya and F. A. Chudnovskii, *Sov. Phys. Tech. Phys.* **32**, 964 (1987) (*Zh. Tekh. Fiz.* **57**, 1617 (1987)).
42. A. I. Gavrilyuk, G. M. Gusinskiĭ and T. G. Lanskaya, *Sov. Tech. Phys. Lett.* **20**, 295 (1994) (*Pis'ma Zh. Tekh. Fiz.* **20**, 77 (1994)).
43. A. I. Gavrilyuk, *Electrochim. Acta* **44**, 3027 (1999).
44. P. Gérard, A. Deneuville and R. Courths, *Thin Solid Films* **71**, 221 (1980).
45. G. Hollinger, T. M. Duc and A. Deneuville, *Phys. Rev. Lett.* **37**, 1564 (1976).
46. S. Hotchandani, I. Bedja, R. W. Fessenden and P. V. Kamat, *Langmuir* **10**, 17 (1994).
47. E. Kikuchi, K. Iida, A. Fujishima and K. Itoh, *J. Electroanal. Chem.* **351**, 105 (1993).
48. E. Kikuchi, N. Hirota, A. Fujishima, K. Itoh and M. Murabayashi, *J. Electroanal. Chem.* **381**, 15 (1995).
49. T. Kubo, Y. Nishikitani, N. Kuroda and M. Matsuno, *Jpn. J. Appl. Phys. Part 1* **35**, 5361 (1996).
50. V. I. Kukuyev, L. F. Komolova, M. V. Lesovoy and Y. Y. Tomaspolsky, *J. Microsc. Spectrosc. Electron.* **14**, 471 (1989).
51. S. T. Li and M. S. El-Shall, *Nanostruct. Mater.* **12**, 215 (1999).
52. S. T. Li, I. N. Germanenko and M. S. El-Shall, *J. Cluster Sci.* **10**, 533 (1999).
53. B. H. Loo, J. N. Yao, H. D. Coble, K. Hashimoto and A. Fujishima, *Appl. Surf. Sci.* **81**, 175 (1994).
54. Y. G. Mo, R. O. Dillon and P. G. Snyder, *J. Vac. Sci. Technol. A* **17**, 2933 (1999).
55. I. E. Obvintseva, M. I. Yanovskaya and R. R. Shifrina, *Inorg. Mater.* **25**, 1530 (1989).
56. V. A. Pilipovich, B. A. Budkevich, V. L. Malevich, I. M. Romanov and I. A. Ges, *Dokl. Akad. Nauk. Belarus.* **27**, 20 (1983) (in Russian).
57. V. A. Pilipovich, B. A. Budkevich, I. M. Romanov, G. D. Ivlev, I. A. Ges and S. P. Zhvavyi, *Phys. Stat. Sol. A* **89**, 709 (1985).
58. H. Qiu and Y. F. Lu, *Jpn. J. Appl. Phys. Part 1* **39**, 5889 (2000).
59. J. C. Santato, M. Ulmann and J. Augustynski, *Adv. Mater.* **13**, 511 (2001).
60. Y. Shigesato, *Jpn. J. Appl. Phys.* **30**, 1457 (1991).
61. L. Y. Su, J. Fang and Z. H. Lu, *Mater. Chem. Phys.* **51**, 85 (1997).
62. L. Y. Su and Z. H. Lu, *Appl. Spectrosc.* **51**, 1587 (1997).
63. L. Y. Su, L. G. Zhang, J. H. Fang, M. H. Xu and Z. H. Lu, *Solar Energ. Mater. Solar Cells* **58**, 133 (1999).
64. L. Y. Su, Q. Dai and Z. H. Lu, *Spectrochim. Acta A* **55**, 2179 (1999).
65. M. Sun, N. Xu, Y. W. Cao, J. N. Yao and E. G. Wang, *J. Mater. Res.* **15**, 927 (2000).
66. M. Sun, N. Xu, Y. W. Cao, J. N. Yao and E. G. Wang, *J. Mater. Sci. Lett.* **19**, 1407 (2000).
67. N. Xu, M. Sun, Y. W. Cao, J. N. Yao and E. G. Wang, *Appl. Surf. Sci.* **157**, 81 (2000).
68. J. N. Yao, B. H. Loo and A. Fujishima, *Ber. Bunsenges. Phys. Chem.* **94**, 13 (1990).
69. J. N. Yao, *Sci. Found. China* **5**, 30 (1997) (in Chinese).
70. J. N. Yao, *World Sci-Tech. R&D* **20**, 121 (1998) (in Chinese).
71. P. Gérard, A. Deneuville, G. Hollinger and T. M. Duc, *J. Appl. Phys.* **48**, 4252 (1977).
72. P. D. Cikmach, J. J. Kleperis, A. R. Lusis and G. M. Ramâns, *Phys. Stat. Sol. A* **90**, K1 (1985).
73. P. Judeinstein and J. Livage, *J. Mater. Chem.* **1**, 621 (1991).
74. M. I. Yanovskaya, I. E. Obvintseva, V. G. Kessler, B. Sh. Galyamov, S. I. Kucheiko, R. R. Shifrina and N. Ya. Turova, *J. Non-Cryst. Solids* **124**, 155 (1990).
75. M. Fujii, T. Kawai, H. Nakamatsu and S. Kawai, *J. Chem. Soc., Chem. Commun.*, 1428 (1983).
76. I. Bedja, S. Hotchandani and P. V. Kamat, *J. Phys. Chem.* **97**, 11064 (1993).

77. P. Gómez-Romero and N. Casañ-Pastor, *J. Phys. Chem.* **100**, 12448 (1996).
78. P. Gómez-Romero, *Solid State Ionics* **101**, 243 (1997).
79. T. He, Y. Ma, Y. A. Cao, X. L. Hu, H. M. Liu, G. J. Zhang, W. S. Yang and J. N. Yao, *J. Phys. Chem. B* **106**, 12670 (2002).
80. Y. P. He, Z. Y. Wu, L. M. Fu, C. R. Li, Y. M. Miao, L. Cao, H. M. Fan and B. S. Zou, *Chem. Mater.* **15**, 4039 (2003).
81. P. V. Kamat, I. Badja and S. Hotochandani, *J. Phys. Chem.* **98**, 9137 (1994).
82. M. T. Nenadović, T. Rajh, O. I. Mićić and A. J. Nozik, *J. Phys. Chem.* **88**, 5827 (1984).
83. K. Vinodgopal, I. Bedja, S. Hotchandani and P. V. Kamat, *Langmuir* **10**, 1767 (1994).
84. C. Sol and R. J. D. Tilley, *J. Mater. Chem.* **11**, 815 (2001).
85. R. J. D. Tilley, *J. Mater. Chem.* **9**, 259 (1999).
86. Y. Zhao, Z. C. Feng, Y. Liang and H. W. Sheng, *Appl. Phys. Lett.* **71**, 2227 (1997).
87. Y. Zhao, Z. C. Feng and Y. Liang, *Acta Phys. Sin.* **7**, 618 (1998).
88. H. D. Dow and D. Redfield, *Phys. Rev.* **8**, 3358 (1970).
89. B. W. Faughnan, R. S. Crandall and P. M. Heyman, *RCA Rev.* **36**, 177 (1975).
90. A. E. Hughes and B. Henderson, in: *Point Defects in Solids*, J. H. Crawford, Jr. and L. M. Slifkin (Eds), Vol. 1, p. 435. Plenum Press, New York, NY (1972).
91. B. W. Faughnan and R. S. Crandall, *Top. Appl. Phys*. **40**, 181 (1980).
92. O. F. Schirmer, V. Wittwer, G. Baur and G. Brandt, *J. Electrochem. Soc.* **124**, 749 (1977).
93. N. F. Mott and E. A. Davis, *Electronic Processes in Non-Crystalline Materials*, 2nd edn. Oxford University Press, Oxford (1979).
94. N. F. Mott, *Metal-Insulator Transitions*, 2nd edn. Taylor and Francis, London (1990).
95. M. L. Hitchman, *J. Electroanal. Chem.* **85**, 135 (1977).
96. J. G. Zhang, D. K. Benson, C. E. Tracy, S. K. Deb, A. W. Czanderna and C. Bechinger, *J. Electrochem. Soc.* **144**, 2022 (1997).
97. E. Salje, A. F. Carley and M. W. Roberts, *J. Solid State Chem.* **29**, 237 (1979).
98. S. K. Deb, *Phys. Rev. B* **16**, 1020 (1977).
99. A. Deneuville, P. Gerard and B. K. Chakraverty, *J. Electron. Mater.* **6**, 747 (1977).
100. I. F. Chang, B. L. Gilbert and T. I. Sun, *J. Electrochem. Soc.* **122**, 955 (1975).
101. E. Ozkan, S. H. Lee, C. E. Tracy, J. R. Pitts and S. K. Deb, *Solar Energ. Mater. Solar Cells* **79**, 439 (2003).
102. R. F. Howe and M. Grätzel, *J. Phys. Chem.* **89**, 4495 (1985).
103. N. M. Dimitrijević, D. Savić, O. I. Mićić and A. J. Nozik, *J. Phys. Chem.* **88**, 4278 (1984).
104. K. Seeger (Ed.), in: *Semiconductor Physics: An Introduction*, p. 343. Springer, Berlin (1982).
105. U. Kölle, J. Moser and M. Grätzel, *Inorg. Chem.* **24**, 2253 (1985).
106. U. Tritthart, A. Gavrilyuk and W. Gey, *Solid State Commun.* **105**, 653 (1998).
107. U. Tritthart, W. Gey and A. Gavrilyuk, *Electrochim. Acta* **44**, 3039 (1999).
108. G. Blasse and A. F. Corsmit, *J. Solid State Chem.* **6**, 513 (1973).
109. W. C. Dautremont-Smith, M. Green and K. S. Kang, *Electrochim. Acta* **22**, 751 (1977).
110. M. T. Pope and G. M. Varga, Jr., *Inorg. Chem.* **5**, 1249 (1966).
111. Y. Kayanuma, *Phys. Rev. B* **38**, 9797 (1988).
112. N. Yoshiike and S. Kondo, *J. Electrochem. Soc.* **130**, 2283 (1983).
113. H. R. Zeller and H. U. Beyeler, *Appl. Phys.* **13**, 231 (1977).
114. Y. Shigesato, A. Murayama, T. Kamimori and K. Matsuhiro, *Appl. Surf. Sci.* **33/34**, 804 (1988).
115. P. Schlotter and L. Pickelmann, *J. Electron. Mater.* **11**, 207 (1982).
116. R. Hurditch, *Electron. Lett.* **11**, 142 (1975).
117. J. Vondrák and J. Bludská, *Solid State Ionics* **68**, 317 (1994).
118. W. C. Conner, G. M. Pajonk and S. J. Teichner, *Adv. Catal.* **34**, 1 (1986).
119. Y. Aikawa, N. Nishimura and M. Sukigara, *Denki Kagaku* **52**, 853 (1984).
120. A. J. Bard and M. S. Wrighton, *J. Electrochem. Soc.* **124**, 1706 (1977).
121. N. Nishimura, Y. Aikawa and M. Sukigara, *Nippon Shashin Kaishi* **48**, 421 (1985).

122. Á. Vértes and R. Schiller, *J. Appl. Phys.* **54**, 199 (1983).
123. T. He, Y. Ma, Y. A. Cao, Y. H. Yin, W. S. Yang and J. N. Yao, *Appl. Surf. Sci.* **180**, 336 (2001).
124. T. He and J. N. Yao, *J. Photochem. Photobiol. C* **4**, 125 (2003).
125. Y. A. Yang, Y. W. Cao, P. Chen, B. H. Loo and J. N. Yao, *J. Phys. Chem. Solids* **59**, 1667 (1998).
126. P. F. Carcia and E. M. McCarron III, *Thin Solid Films* **155**, 53 (1987).
127. J. Scarminio, A. Lourenço and A. Gorenstein, *Thin Solid Films* **302**, 66 (1997).
128. M. R. Tubbs, *Phys. Stat. Sol. A* **21**, 253 (1974).
129. F. A. Chudnovskii, D. M. Schaefer, A. I. Gavrilyuk and R. Reifenberger, *Appl. Surf. Sci.* **62**, 145 (1992).
130. M. Anwar and C. A. Hogarth, *Phys. Stat. Sol. A* **109**, 469 (1988).
131. M. Anwar, C. A. Hogarth and K. Lott, *J. Mater. Sci.* **24**, 1660 (1989).
132. M. Anwar, C. A. Hogarth and C. R. Theocharis, *J. Mater. Sci.* **24**, 2387 (1989).
133. M. Anwar, C. A. Hogarth and R. Bulpett, *J. Mater. Sci.* **24**, 3087 (1989).
134. M. Anwar and C. A. Hogarth, *Int. J. Electron.* **67**, 567 (1989).
135. J. W. Rabalais, R. J. Colton, A. M. Guzman, *Chem. Phys. Lett.* **29**, 131 (1974).
136. C. Julien, A. Khelfa, O. M. Hussain and G. A. Nazri, *J. Cryst. Growth* **156**, 235 (1995).
137. A. F. Jankowski and L. R. Schrawyer, *Thin Solid Films* **193**, 61 (1990).
138. T. C. Arnoldussen, *J. Electrochem. Soc.* **123**, 527 (1976).
139. F. Kumada, M. Okamoto, M. Baba and T. Ikeda, *Jpn. J. Appl. Phys.* **25**, L574 (1986).
140. A. Abdellaoui, L. Martin and A. Donnadieu, *Phys. Stat. Sol. A* **109**, 455 (1988).
141. A. Abdellaoui, G. Lévêque, A. Donnadieu, A. Bath and B. Bouchikhi, *Thin Solid Films* **304**, 39 (1997).
142. J. S. Cross and G. L. Schrader, *Thin Solid Films* **259**, 5 (1995).
143. X. H. Ji, Y. A. Yang and J. N. Yao, *Photograph. Sci. Photochem.* **16**, 353 (1998) (in Chinese).
144. Y. Z. Zhang, Y. S. Huang, Y. Z. Cao, S. L. Kuai and X. F. Hu, *Acta Chim. Sin.* **59**, 2076 (2001).
145. J. N. Yao, B. H. Loo, K. Hashimoto and A. Fujishima, *J. Electroanal. Chem.* **290**, 263 (1990).
146. J. N. Yao, P. Chen and A. Fujishima, *Photograph. Sci. Photochem.* **14**, 224 (1996) (in Chinese).
147. D. Guay, G. Tourillon, G. Laperriere and D. Belanger, *J. Phys. Chem.* **96**, 7718 (1992).
148. O. M. Hussain, K. S. Rao, K. V. Madhuri, C. V. Ramana, B. S. Naidu, S. Pai, J. John and R. Pinto, *Appl. Phys. A* **75**, 417 (2002).
149. V. A. Ioffe, I. B. Patrina, E. V. Zelenetskaya and V. P. Mikheeva, *Phys. Stat. Sol.* **35**, 535 (1969).
150. R. S. Mann and K. C. Khulbe, *Bull. Chem. Soc. Jpn.* **48**, 1021 (1975).
151. E. Serwicka, *J. Solid State Chem.* **51**, 300 (1984).
152. H. J. Wagner, P. Driessen and C. F. Schwerdtfeger, *J. Non-Crystal. Solids* **34**, 335 (1979).
153. R. J. Colton, A. M. Guzman and J. W. Rabalais, *J. Appl. Phys.* **49**, 409 (1978).
154. J. J. Birtill and P. G. Dickens, *Mater. Res. Bull.* **13**, 311 (1978).
155. P. G. Dickens, J. J. Birtill and C. J. Wright, *J. Solid State Chem.* **28**, 185 (1979).
156. M. N. Mondragón, O. Zelaya-Angel, R. Ramírez-Bon, J. L. Herrera and C. Reyes-Betanzo, *Physica B* **271**, 369 (1999).
157. P. Pichat, M. Mozzanega and C. Hoang-Van, *J. Phys. Chem.* **92**, 467 (1988).
158. G. S. Nadkarni and J. G. Simmons, *J. Appl. Phys.* **41**, 545 (1970).
159. K. Ajito, L. A. Nagahara, D. A. Tryk, K. Hashimoto and A. Fujishima, *J. Phys. Chem.* **99**, 16383 (1995).
160. K. Eda, *J. Solid State Chem.* **98**, 350 (1992).
161. Y. A. Yang, Y. W. Cao, B. H. Loo and J. N. Yao, *J. Phys. Chem. B* **102**, 9392 (1998).
162. M. S. Jagadeesh and V. D. Das, *J. Non-Cryst. Solids* **28**, 327 (1978).
163. T. Maruyama and T. Kanagawa, *J. Electrochem. Soc.* **142**, 1644 (1995).
164. N. Miyata, T. Suzuki and R. Ohyama, *Thin Solid Films* **281/282**, 218 (1996).
165. V. K. Sabhapathi, O. M. Hussain. P. S. Reddy, K. T. T. Reddy, S. Uthanna, B. S. Naidu and P. J. Reddy, *Phys. Stat. Sol. A* **148**, 167 (1995).

166. A. I. Gavrilyuk, A. A. Mansurov, A. Kh. Razikov, F. A. Chudnovskii and I. Kh. Shaver, *Sov. Phys. Tech. Phys.* **31**, 585 (1986) (*Zh. Tekh. Fiz.* **56**, 958 (1986)).
167. T. He, Y. Ma, Y. A. Cao, P. Jiang, X. T. Zhang, W. S. Yang and J. N. Yao, *Langmuir* **17**, 8024 (2001).
168. A. I. Gavrilyuk, A. A. Mansurov and F. A. Chudnovskii, *Sov. Tech. Phys. Lett.* **10**, 292 (1984) (*Pis'ma Zh. Tekh. Fiz.* **10**, 693 (1984)).
169. A. I. Gavrilyuk, G. M. Gusinskii, A. A. Mansurov, L. A. Rassadin and F. A. Chudnovskii, *Sov. Phys. Solid State* **28**, 1147 (1986) (*Fiz. Tverd. Tela (Leningrad)* **28**, 2053 (1986)).
170. J. N. Yao, *Photograph. Sci. Photochem.* **15**, 363 (1997) (in Chinese).
171. J. N. Yao, Y. A. Yang and B. H. Loo, *J. Phys. Chem. B* **102**, 1856 (1998).
172. J. N. Yao and B. H. Loo, *Solid State Commun.* **105**, 479 (1998).
173. J. N. Yao, B. H. Loo, K. Hashimoto and A. Fujishima, *Ber. Bunsenges. Phys. Chem.* **95**, 557 (1991).
174. B. W. Faughnan, D. L. Staebler and Z. J. Kiss, *Appl. Solid State Sci.* **2**, 107 (1971).
175. D. Duonghong, J. Ramsden and M. Grätzel, *J. Am. Chem. Soc.* **104**, 2977 (1982).
176. A. Henglein, *Ber. Bunsen-Ges. Phys. Chem.* **86**, 241 (1982).
177. J. S. Huang, H. L. Ding, W. S. Dodson and Y. Z. Li, *Anal. Chim. Acta* **311**, 115 (1995).
178. C. Kormann, D. W. Bahnemann and M. R. Hoffmann, *J. Phys. Chem.* **92**, 5196 (1988).
179. G. Rothenberger, J. Moser, M. Grätzel, N. Serpone and D. K. Sharma, *J. Am. Chem. Soc.* **107**, 8054 (1985).
180. N. Serpone, D. Lawless, R. Khairutdinov and E. Pelizzetti, *J. Phys. Chem.* **99**, 16655 (1995).
181. D. E. Skinner, D. P. J. Columbo, J. J. Calvieri and R. M. Bowmann, *J. Phys. Chem.* **99**, 7853 (1995).
182. M. P. Zheng, M. Y. Gu, Y. P. Jin and G. L. Jin, *J. Mater. Sci. Lett.* **20**, 485 (2001).
183. M. P. Zheng, Y. P. Jin, G. L. Jin, M. Y. Gu and P. Tao, *Acta Chim. Sin.* **59**, 142 (2001).
184. F. N. Castellano, J. M. Stipkala, L. A. Friedman and G. J. Meyer, *Chem. Mater.* **6**, 2123 (1994).
185. Z. S. Guan, Y. Ma, Y. A. Cao, X. H. Ji and J. N. Yao, *Acta Phys. Chim. Sin.* **16**, 5 (2000).
186. T. Matsumoto, Y. Murakami and Y. Takasu, *Chem. Lett.*, 348 (2000).
187. J. G. Highfield and M. Grätzel, *J. Phys. Chem.* **92**, 464 (1988).
188. T. Torimoto, R. J. Fox III and M. A. Fox, *J. Electrochem. Soc.* **143**, 3712 (1996).
189. L. Y. Su and Z. H. Lu, *J. Photochem. Photobiol. A: Chem.* **107**, 245 (1997).
190. D. Bahnemann, A. Henglein, J. Lilie and L. Spanhel, *J. Phys. Chem.* **88**, 709 (1984).
191. A. K. Ghosh, F. G. Wakim and R. R. Addiss, Jr., *Phys. Rev.* **184**, 979 (1969).
192. K. J. Kim, K. D. Benkstein, J. van de Lagemaat and A. J. Frank, *Chem. Mater.* **14**, 1042 (2002).
193. O. I. Micic, Y. N. Zhang, K. R. Cromack, A. D. Trifunac and M. C. Thurnauer, *J. Phys. Chem.* **97**, 13284 (1993).
194. M. Grätzel and R. F. Howe, *J. Phys. Chem.* **94**, 2566 (1990).
195. A. Talledo, C. G. Granqvist, *J. Appl. Phys.* **77**, 4655 (1995).
196. A. I. Gavrilyuk and T. G. Lanskaya, *Sov. Tech. Phys. Lett.* **20**, 219 (1994). (*Pis'ma Zh. Tekh. Fiz.* **20**, 12 (1994)).
197. S. Nishio and M. Kakihana, *Chem. Mater.* **14**, 3730 (2002).
198. S. Nishio, M. Kakihana, H. Eba and K. Sakurai, *Jpn. J. Appl. Phys.* **42**, 5670 (2003).
199. N. Kenny, C. R. Kannewurf and D. H. Whitmore, *J. Phys. Chem. Solids* **27**, 1237 (1966).
200. C. V. Ramana, O. M. Hussain, B. S. Naidu and P. J. Reddy, *Thin Solid Films* **305**, 219 (1997).
201. J. N. Yao, B. H. Loo, K. Hashimoto and A. Fujishima, *Ber. Bunsenges. Phys. Chem.* **95**, 554 (1991).
202. J. N. Yao, B. H. Loo, K. Hashimoto and A. Fujishima, *Ber. Bunsenges. Phys. Chem.* **96**, 699 (1992).
203. P. V. Kamat and B. Patrick, *J. Phys. Chem.* **96**, 6829 (1992).
204. U. Koch, A. Fojtik, H. Weller and A. Henglein, *Chem. Phys. Lett.* **122**, 507 (1985).
205. M. Matsuoka and K. Ono, *Appl. Phys. Lett.* **53**, 1393 (1988).

206. Z. H. Chen, Y. Ma, T. He, R. M. Xie, K. Shao, W. S. Yang and J. N. Yao, *New J. Chem.* **26**, 621 (2002).
207. S. H. Elder, F. M. Cot, Y. Su, S. M. Heald, A. M. Tyryshkin, M. K. Bowman, Y. Gao, A. G. Joly, M. L. Balmer, A. C. Kolwaite, K. A. Magrini and D. M. Blake, *J. Am. Chem. Soc.* **122**, 5138 (2000).
208. P. Judeinstein, P. W. Oliverira, H. Krug and H. Schmidt, *Adv. Mater. Opt. Electr.* **7**, 123 (1997).
209. G. J. Zhang, T. He, Y. Ma, Z. H. Chen, W. S. Yang and J. N. Yao, *Phys. Chem. Chem. Phys.* **5**, 2751 (2003).
210. T. R. Zhang, W. Feng, Y. Q. Fu, R. Lu, C. Y. Bao, X. T. Zhang, B. Zhao, C. Q. Sun, T. J. Li, Y. Y. Zhao and J. N. Yao, *J. Mater. Chem.* **12**, 1453 (2002).